JOURNAL OF SYNCHROTRON RADIATION
ISSN 1600-5775

Implementation of ultrafast X-ray diffraction at the 1W2B wiggler beamline of Beijing Synchrotron Radiation Facility

Da-Rui Sun,[a] Guang-Lei Xu,[b] Bing-Bing Zhang,[a] Xue-Yan Du,[a] Hao Wang,[a] Qiu-Ju Li,[a] Yang-Fan Zhou,[a] Zhen-Jie Li,[a] Yan Zhang,[a] Jun He,[b] Jun-Hui Yue,[b] Ge Lei[b] and Ye Tao[a]*

[a]Beijing Synchrotron Radiation Facility, Institute of High Energy Physics, Chinese Academy of Sciences, 19B Yuquan Road, Beijing 100049, People's Republic of China, and [b]Accelerator Division, Institute of High Energy Physics, Chinese Academy of Sciences, 19B Yuquan Road, Beijing 100049, People's Republic of China. *Correspondence e-mail: taoy@ihep.ac.cn

Received 13 January 2016
Accepted 13 March 2016

Edited by J. F. van der Veen

Keywords: laser pump/X-ray probe; ultrafast X-ray diffraction; photo-induced strain.

The implementation of a laser pump/X-ray probe scheme for performing picosecond-resolution X-ray diffraction at the 1W2B wiggler beamline at Beijing Synchrotron Radiation Facility is reported. With the hybrid fill pattern in top-up mode, a pixel array X-ray detector was optimized to gate out the signal from the singlet bunch with interval 85 ns from the bunch train. The singlet pulse intensity is $\sim 2.5 \times 10^6$ photons pulse^{-1} at 10 keV. The laser pulse is synchronized to this singlet bunch at a 1 kHz repetition rate. A polycapillary X-ray lens was used for secondary focusing to obtain a 72 µm (FWHM) X-ray spot. Transient photo-induced strain in $BiFeO_3$ film was observed at a $\sim$150 ps time resolution for demonstration.

1. Introduction

The significance could not be overestimated if we were able to capture the structure change in a chemical or physical process, since dynamic structure information is imperative to unravelling the mechanism and bridge between structure and function. Synchrotrons have played an important role in ultrafast X-ray studies based on the laser pump/X-ray probe scheme, which has been realised at several synchrotron sources (Kozina *et al.*, 2014; Lima *et al.*, 2011; March *et al.*, 2011; Ejdrup *et al.*, 2009; Navirian *et al.*, 2007, 2012; Laulhé *et al.*, 2013). The time resolution is usually dependent on the X-ray pulse duration, which is generally 100 ps (FWHM) for synchrotron lightsources, while the laser-slicing technique has been developed to obtain a femtosecond pulse but at the large expense of pulse intensity (Beaud *et al.*, 2007). Recently, the X-ray free-electron laser has transformed dynamic research owing to its <100 fs pulse and unprecedented pulse intensity (Chollet *et al.*, 2015). However, for dynamic studies in the picosecond to microsecond range, the synchrotron has its advantages due to its excellent stability, broader energy tune range and higher repetition rate.

The Beijing Synchrotron Radiation Facility (BSRF) is a parasitic light source of the Beijing Electron and Positron Collider. Here we describe the implementation of the laser pump/X-ray probe system at BSRF under hybrid fill pattern, utilizing a 1 kHz laser system and a gated pixel array X-ray detector. The photo-induced lattice dynamics in $BiFeO_3$ film were investigated by picosecond X-ray diffraction to demonstrate the capability of the setup.

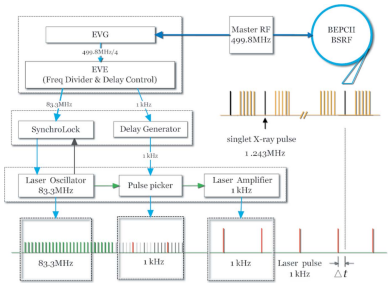

2. Experimental details

Like ultrafast optical and electron measurements, ultrafast X-ray methods generally employ a pump–probe scheme. A pulse, usually a laser pulse, excites a sample to excitation state and a following X-ray pulse arrives at a fixed timing delay to snapshot the structure at this moment. The complete dynamic process is revealed by recording at different delays between the X-ray and the laser pulse. The details of our laser pump/X-ray probe setup are described in this section.

2.1. X-ray source

The laser pump/X-ray probe experiment generally requires a hybrid fill pattern in which a specific single bunch is filled with sufficient interval from other bunches such that the signal from the singlet can be selected out. The hybrid fill pattern has become a routine fill mode in BSRF operation. As shown in Fig. 1, the interval between the singlet bunch and bunch train is 85 ns. The X-ray pulse from this singlet bunch will be synchronized with the laser pulse and captured by the detector. The storage ring was operating in top-up mode with a constant beam current at 250 mA and singlet bunch current at 1.6 mA. The X-ray pulse intensity from this singlet is $\sim 2.5 \times 10^6$ photons pulse^{-1} at 10 keV. The X-ray pulse duration is $\sim$150 ps (FWHM), calculated from the bunch length. This singlet bunch circulates around the storage ring at 1.243 MHz with a period of 804 ns.

The laser beam was guided to the 1W2B beamline, a wiggler beamline at BSRF. A Si(111) double-crystal monochromator provides an energy tuning range from 5 keV to 15 keV with energy resolution $\Delta E/E = 4 \times 10^{-4}$. A toroidal mirror focuses the beam to 0.8 mm (V) $\times$ 1.0 mm (H) (FWHM). To excite the sample efficiently and uniformly, the size of the laser spot is required to be larger than the X-ray spot on the sample. A small laser spot is helpful in mitigating the heating effect and reducing sample damage; thus, a smaller X-ray spot size is preferred. A polycapillary lens was used as a secondary focusing optics due to its large acceptance and ease of installation and alignment. The lens can focus the X-ray beam down to 72 µm (FWHM). Although the beam angular divergence increases after the capillary lens, it can be utilized to enable the sample multiple diffraction peaks and substrate signal to be observable simultaneously if an area X-ray detector was used. The substrate signal can be used as a reference signal for normalization, which is imperative in detecting a diffraction intensity change. Further, the simultaneously observed multiple peaks will keep the detection of the change of different diffraction peaks consistent, and improve time-resolved experiment efficiency.

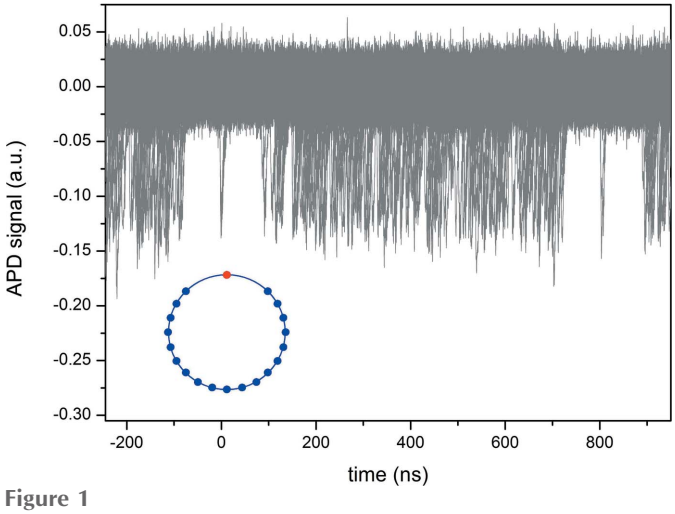

Figure 1
Bunch structure measured by avalanche photodiode (APD). Inset: schematic of the hybrid bunch structure, with the singlet bunch in red. The interval between this singlet bunch and the bunch trains (blue) is 85 ns.

2.2. Laser source

The femtosecond laser, equipped for our established laser plasma X-ray source, is shared as the pump source for the synchrotron-based pump–probe setup. The laser system consists of a Ti:sapphire oscillator (Micra5, Coherent Ltd) and a Ti:sapphire regenerative amplifier (Legend Elite USP He+, Coherent Ltd). The oscillator operates at 83.3 MHz repetition rate, one-sixth of the storage-ring radio frequency (RF) 499.8 MHz. The synchronization between the laser pulse and the X-ray pulse was realised in the oscillator, as described in the following section. The laser pulse from the oscillator needs to be amplified by the amplifier for practical application, and thus the repetition rate of the pump–probe measurement is generally dependent on the laser amplifier repetition rate. The amplifier runs at 1.002 kHz repetition rate (1/1240 of the storage-ring revolution frequency 1.243 MHz) with 800 nm fundamental output.

The laser system is located in a temperature-stabilized room for the laser-plasma X-ray source-based pump–probe setup. In order to reach the desired beamline 1W2B, the laser beam is transported for 45 m using mirrors. The laser spot stability at the sample position was kept within 50 µm after transportation. To overcome long-term drift owing to the 45 m transportation path, we installed an active laser feedback unit (MRC Systems GmbH). In addition, the pulse was stretched from 40 fs to $\sim$1 ps for transportation in order to reduce adverse nonlinear effects, while the 1 ps pulse is sufficient for the sample pump with respect to the 100 ps X-ray pulse. In the meantime, the stretched pulse could mitigate the nonlinear optic effects in sample absorption. Close to the sample, a diode was installed to detect the laser leaked from the reflection mirror, and this diode signal will be used in gating detection. The parameters of both the X-ray and the laser source are listed in Table 1.

2.3. Synchronization and delay control

Synchronization between the X-ray pulse and the laser pulse is a prerequisite for the laser pump/X-ray probe system. The timing of the X-ray pulse is determined by the RF signal of the master oscillator. If we use the RF signal as a reference to control the frequency and phase of the laser pulse, the laser pulse will be synchronized to the X-ray pulse. Because the

Table 1
Parameters of the X-ray and laser source.

X-ray source		Laser source	
Energy (keV)	5–15	Wavelength (nm)	800, 400, 266
Energy resolution ($\Delta E/E$)	4×10^{-4}	Maximum pulse energy (mJ)	4 at fundamental
Pulse intensity (photons pulse^{-1})	$\sim 2.5 \times 10^{6}$ at 10 keV	Pulse energy stability in 8 h	<1% r.m.s.
Spot size (FWHM) (μm)	72 at 10 keV	Repetition rate (kHz)	1
Beam time available in hybrid mode	4–5 months annually	Duration (ps)	1
		Spot size (FWHM)	100 μm–1 mm

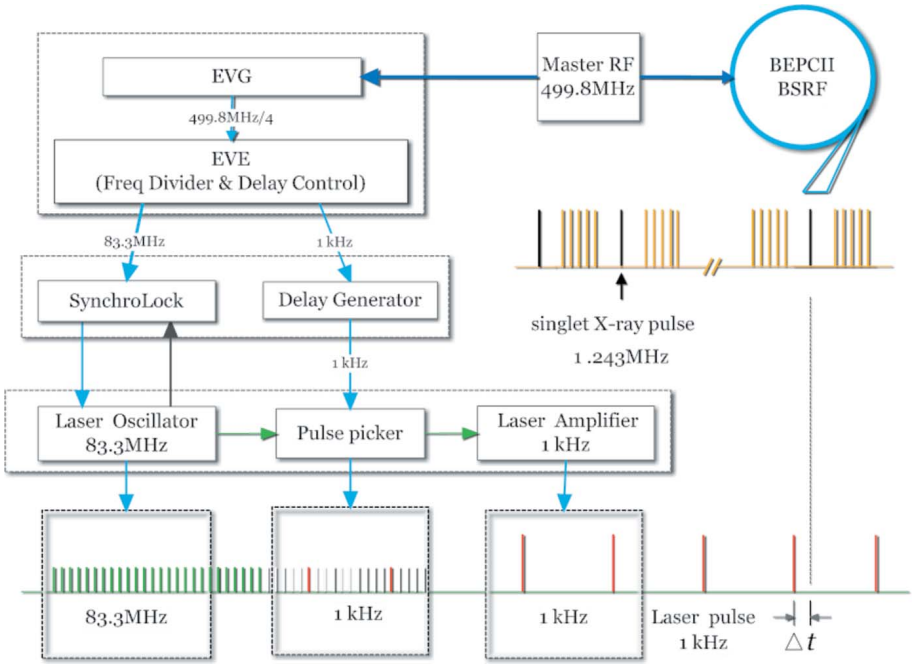

Figure 2
Layout of the timing system design for laser pump/X-ray probe setup, including synchronization and delay control. See text for explanation.

frequency and phase of the laser pulse are determined by the laser oscillator cavity length, by using a piezo-controlled mirror in the oscillator cavity, the cavity length can be adjusted actively to phase lock the reference signal from RF so that the laser pulse is in synchronization with the X-ray pulse.

The synchronization and delay control design is displayed in Fig. 2. The master RF frequency is 499.8 MHz, which was divided into 124.95 MHz by an event generator (EVG), and then distributed by optical fiber to a FPGA-based event electronic module (EVE) and an event receiver (EVR). The EVE is located in the laser room, while the EVR is in the beamline providing a timing trigger. The EVE plays the roles of a frequency divider and fine delay control as well. It down-converted the 124.95 MHz to 83.3 MHz as the reference signal. The reference signal was input into a phase-lock loop unit (SynchroLock; Coherent Ltd), which controlled a pizeo-actuated cavity mirror to phase lock the reference signal. The jitter between the oscillator laser pulse and the reference is 9.9 ps (RMS). After synchronization, the pulses from the oscillator were selected by a pulse picker triggered by a 1.002 kHz signal from the EVE and sent to the laser amplifier.

In order to record dynamic processes, the delay (Δt) between laser and X-ray pulse needs to be adjustable. Delay control was realised in two ways. Because the interval between laser pulses from the oscillator is 12 ns, corresponding to a 83.3 MHz repetition rate, for coarse delay control we could vary the delay at a 12 ns step by picking the alternative pulse from pulse trains of the oscillator output (Fig. 2). Next, fine delay control within 12 ns was achieved by the EVE at a minimum step of 5 ps.

2.4. Temporal and spatial overlap

The X-ray pulse and the laser pulse should be temporally and spatially overlapped for laser pump/X-ray probe measurements. With respect to the coarse temporal overlap, we used an in-house-built avalanche photodiode detector which is sensitive to both X-ray and optical laser pulse with 2 ns rise edge. Monitoring on a 4 GHz oscilloscope, we could observe the interval between X-ray and laser signal. By adjusting the delay between the laser pulse and the X-ray pulse, we could align the half-height position of the rising edges of both the X-ray and the laser signals, as shown in Fig. 3. This alignment could attain temporal overlap within 500 ps. The accurate temporal overlap was optimized by scanning the delay for maximum sample laser-on signal.

For coarse spatial overlap, a thin photographic film sensitive to X-rays was placed on the surface of the sample to expose the X-ray spot. The laser spot is around 800 μm in diameter, much larger than the X-ray spot size, so it was convenient to adjust the laser spot position using a motorized mirror to overlap the exposed X-ray spot. Precise spatial overlap could be achieved by scanning the laser spot on the sample to maximize the sample laser-on signal.

2.5. Gated detection

The interval between the singlet and bunch trains is ~85 ns, as shown in Fig. 4(*a*). However, there is no mechanical chopper fast enough to isolate this singlet pulse with hard

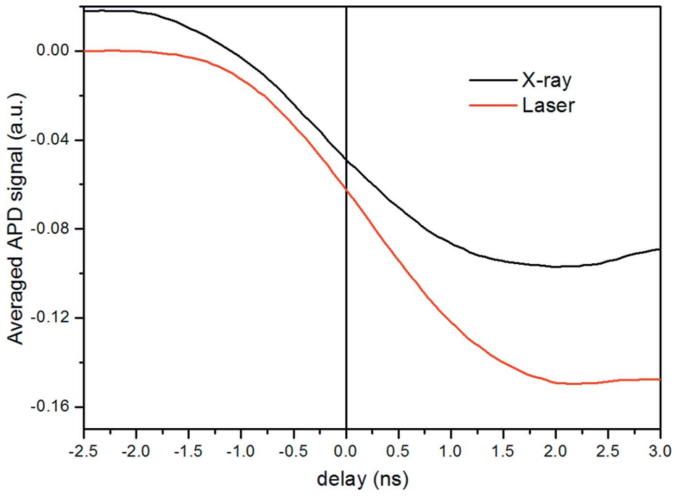

Figure 3
Temporal overlap by alignment of the half-amplitude position of the averaged APD signals from both the X-ray and the laser pulse.

X-rays (Cammarata *et al.*, 2009). To circumvent this limitation, we used an X-ray pixel array detector (Pilatus 100k) for diffraction detection, as its electronic gate function could be utilized to gate out the signal from the singlet pulse (Ejdrup *et al.*, 2009). In addition, the large scan range of the area detector makes it favourable for time-resolved experiments, especially for measurements based on polycapillary focusing. The gate signal width is 10 ns and comes from a delay generator triggered by a 1.002 kHz signal from the EVR, *i.e.* with frequency the same as the laser amplifier repetition rate. This area detector was optimized in energy threshold and apparent gate width to narrow down the effective gate window width for gating out the expected signal. Then we scanned the gated signal through a 804 ns range, the storage-ring revolution period. As shown in Fig. 4(*b*), the integrated scattering signal presents a pattern similar to the hybrid bunch structure in Fig. 1, and the bump around 100 ns represents the signal from the singlet bunch. From this scan the effective gate ability of the detector is estimated to be around 80 ns. The gate was fixed at the bump centre position to gate out the laser-on signal after the temporal overlap was attained. In the meantime, both the analogue exposure output of the detector and the diode signal of the laser pulse were monitored to ensure gating of the laser-on signal.

3. Ultrafast X-ray diffraction demonstration

Diffraction detection was performed in vertical scattering plane geometry. The detector distance was adjustable, up to a maximum of 750 mm. The evacuated tube between the sample and the detector was used to decrease air absorption and served for scattering suppression as well. The sample could be measured down to 100 K using a commercial open-flow nitrogen gas cryostat.

The performance of the laser pump/X-ray probe setup was demonstrated by measuring the photo-induced strain in $BiFeO_3$ (BFO) film, a well studied multiferroic material, by

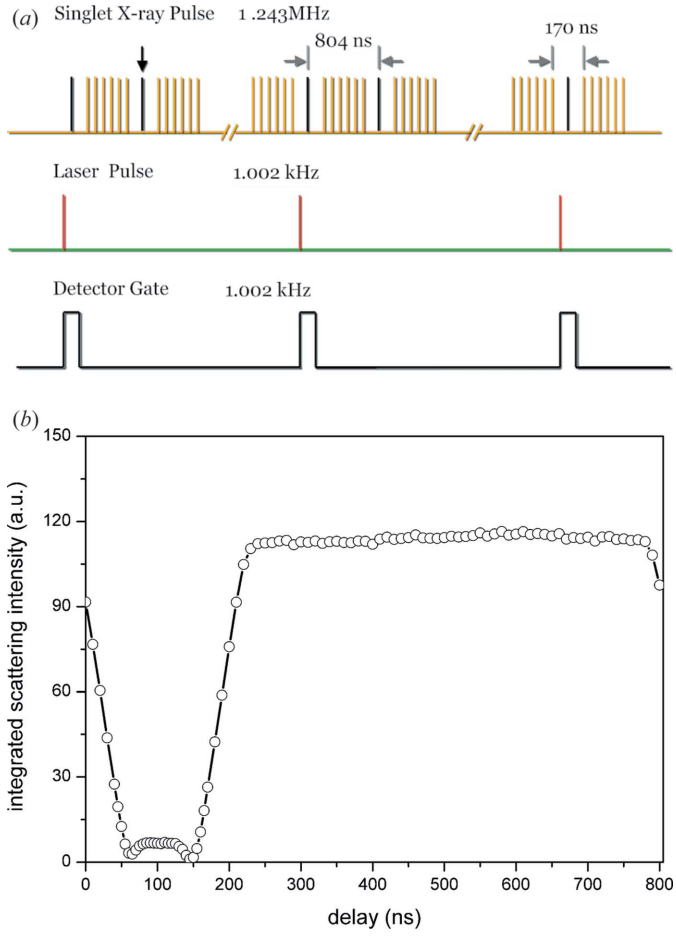

Figure 4
(*a*) Sketch of the detection gate structure. (*b*) The integrated scattering counts as a function of delay scan at 5–10 ns steps. The bump represents the signal from the singlet.

ultrafast X-ray diffraction (Wen *et al.*, 2013; Schick *et al.*, 2014; Li *et al.*, 2015). A 35 nm-thick BFO film was grown onto a $LaSrAlTiO_3$ substrate by reactive molecular-beam epitaxy. Because the optical band gap of BFO is 2.74 eV (Ihlefeld *et al.*, 2008), the 800 nm fundamental laser pulse is frequency doubled by a BBO crystal to 400 nm (3.1 eV) for the electronic excitation. The X-ray flux of the 1W2B beamline peaks at 10 keV, so we selected 10 keV for diffraction. The gated diffraction signal was obtained by the above area detector, which is 415 mm away from the sample. The static diffraction measurements are compared for gated and non-gated signal in Fig. 5(*a*). The ultrafast X-ray diffraction signal was detected by monitoring the Bragg peak of the (002) reflection of the BFO at room temperature. Upon photoexcitation, the (002) peak shifts to lower angle and becomes broader, as shown in Fig. 5(*b*). The shift represents an expansion of the BFO out-of-plane lattice parameter *c*. This transient out-of-plane strain can be attributed to the localized photoinduced carriers and the accompanying change of electric field (Wen *et al.*, 2013). The change of the Bragg angle of the BFO (002) reflection, along with the corresponding photoinduced strain ($\Delta c/c$) and peak width change, is displayed as a function of time delay

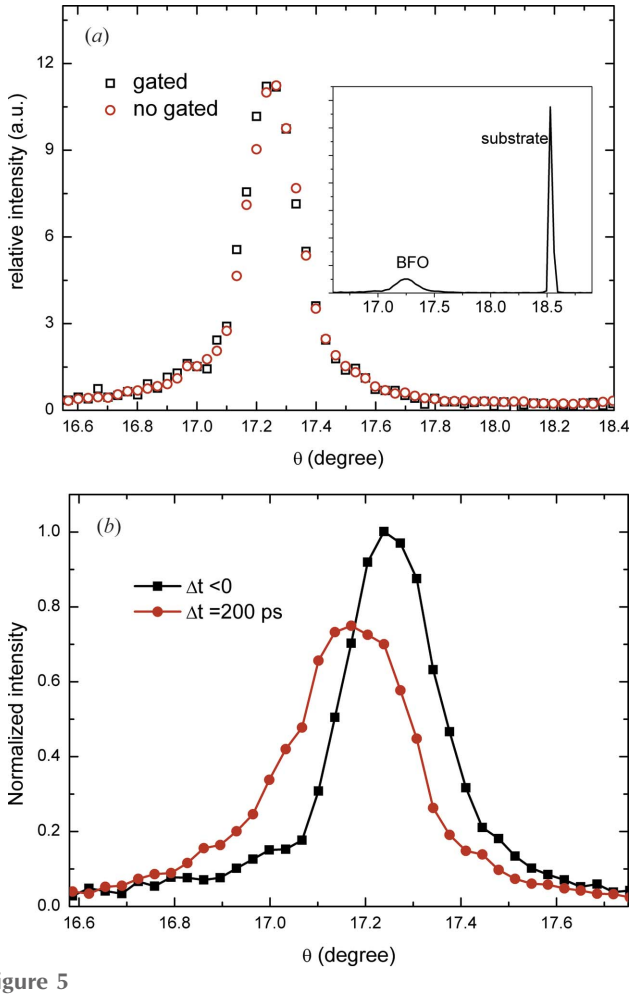

Figure 5
(*a*) Intensity and profile consistence between the gated and the non-gated BFO signal. Black: gated signal intensity at 1 kHz, 10 ns gate width, 30 s exposure, signal multiplied by a factor of 2.2. Red: non-gated signal, 0.01 s exposure with X-ray attenuation by 30 times. Inset: gated diffraction peaks of BFO (002) and substrate recorded simultaneously. (*b*) Rocking curves of BFO (002) peak before ($\Delta t < 0$) (black) and after ($\Delta t = 200$ ps) (red) laser excitation at 1.8 mJ cm^{-2} fluence.

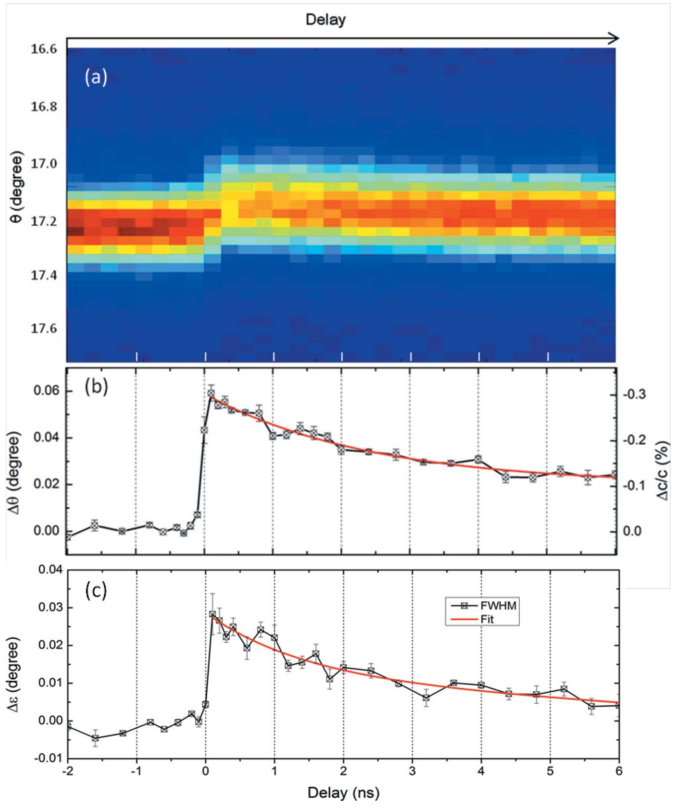

Figure 6
(*a*) Two-dimensional plot of the BFO (002) peak shift upon photoexcitation at 1.8 mJ cm^{-2} fluence. (*b*) Angular shift ($\Delta\theta$) of the (002) peak and the photoinduced strain ($\Delta c/c$) as a function of delay up to 6 ns at the minimum delay step 100 ps. The red line represents the fit using a single component exponential function. (*c*) Width (FWHM) change of the 002 peak as a function of delay.

in Fig. 6. The relaxation process of the angle shift and peak broadening can be fitted by a single component exponential function with a time constant of 2.4 ns and 1.9 ns, respectively, consistent with that reported (Wen *et al.*, 2013).

4. Summary and outlook

We have implemented a laser pump/X-ray probe scheme in a wiggler beamline at BSRF and observed photo-induced strain in a BFO film at ∼150 ps resolution. There is room for improvement in the jitter suppression and the signal-to-noise ratio. The jitter between laser and RF signal will be improved after upgrade of our RF distribution system. The singlet bunch current is only 1.6 mA, but it could be increased to at least 5 mA in the near future to provide a higher pulse intensity for ultrafast detection. Moreover, the current setup runs at 1 kHz repetition rate due to laser repetition rate limitation. The revolution frequency of the singlet bunch is 1.243 MHz, so a high-repetition-rate pump–probe, up to MHz, will be developed using a high-repetition-rate laser (Kozina *et al.*, 2014; Lima *et al.*, 2011; March *et al.*, 2011; Navirian *et al.*, 2012). The current Pilatus 100k detector can run under gate mode triggered at 1.24 MHz to capture the singlet signal. Compared with 1 kHz rate collection, the data quality collected under MHz rate is expected to be improved remarkably. Furthermore, the MHz laser will be portable, so the laser pump/X-ray probe system will be available at other beamlines. Besides diffraction detection, the probe will be extended to X-ray absorption/emission spectroscopy and liquid scattering.

In addition, we have established a sub-picosecond laser pump/X-ray probe ultrafast X-ray diffraction setup based on a table-top laser plasma femtosecond X-ray source (Zhang *et al.*, 2014). However, the laser plasma source has limitations in intensity stability, pulse intensity and fixed energy at the Cu $K\alpha$ line. Excepting pulse duration, the synchrotron X-ray source has advantages over these limitations. Therefore, these two methods are complementary in ultrafast detection, and this synergy has been applied well elsewhere (Schick *et al.*, 2014). In combination with laser plasma source-based sub-picosecond detection, the implementation of synchrotron-based time-resolved X-ray detection will make the BSRF a first-generation parasitic lightsource with unique capability in ultrafast X-ray study.

Acknowledgements

The BFO sample was kindly provided by Dr Yuelin Li, Advanced Photon Source. We are grateful to Zhenhua Gao and Yinglei Tan for their help with software and hardware setup. This work is supported by the High Energy Photon Source-Test Facility project and the National Science Foundation of China (U1332205).

References

Beaud, P., Johnson, S. L., Streun, A., Abela, R., Abramsohn, D., Grolimund, D., Krasniqi, F., Schmidt, T., Schlott, V. & Ingold, G. (2007). *Phys. Rev. Lett.* **99**, 174801.

Cammarata, M., Eybert, L., Ewald, F., Reichenbach, W., Wulff, M., Anfinrud, P., Schotte, F., Plech, A., Kong, Q. Y., Lorenc, M., Lindenau, B., Räbiger, J. & Polachowski, S. (2009). *Rev. Sci. Instrum.* **80**, 015101.

Chollet, M., Alonso-Mori, R., Cammarata, M., Damiani, D., Defever, J., Delor, J. T., Feng, Y., Glownia, J. M., Langton, J. B., Nelson, S., Ramsey, K., Robert, A., Sikorski, M., Song, S., Stefanescu, D., Srinivasan, V., Zhu, D., Lemke, H. T. & Fritz, D. M. (2015). *J. Synchrotron Rad.* **22**, 503–507.

Ejdrup, T., Lemke, H. T., Haldrup, K., Nielsen, T. N., Arms, D. A., Walko, D. A., Miceli, A., Landahl, E. C., Dufresne, E. M. & Nielsen, M. M. (2009). *J. Synchrotron Rad.* **16**, 387–390.

Ihlefeld, J. F., Podraza, N. J., Liu, Z. K., Rai, R. C., Xu, X., Heeg, T., Chen, Y. B., Li, J., Collins, R. W., Musfeldt, J. L., Pan, X. Q., Schubert, J., Ramesh, R. & Schlom, D. G. (2008). *Appl. Phys. Lett.* **92**, 142908.

Kozina, M., Hu, T., Wittenberg, J. S., Szilagyi, E., Trigo, M., Miller, T. A., Uher, C., Damodaran, A., Martin, L., Mehta, A., Corbett, J., Safranek, J., Reis, D. A. & Lindenberg, A. M. (2014). *Struct Dyn.* **1**, 034301.

Laulhé, C., Cammarata, M., Servol, M., Miller, R. J. D., Hada, M. & Ravy, S. (2013). *Eur. Phys. J. Spec. Top.* **222**, 1277–1285.

Li, Y., Adamo, C., Chen, P., Evans, P. G., Nakhmanson, S. M., Parker, W., Rowland, C. E., Schaller, R. D., Schlom, D. G., Walko, D. A., Wen, H. & Zhang, Q. (2015). *Sci. Rep.* **5**, 16650.

Lima, F. A., Milne, C. J., Amarasinghe, D. C. V., Rittmann-Frank, M. H., van der Veen, R. M., Reinhard, M., Pham, V. T., Karlsson, S., Johnson, S. L., Grolimund, D., Borca, C., Huthwelker, T., Janousch, M., van Mourik, F., Abela, R. & Chergui, M. (2011). *Rev. Sci. Instrum.* **82**, 063111.

March, A. M., Stickrath, A., Doumy, G., Kanter, E. P., Krässig, B., Southworth, S. H., Attenkofer, K., Kurtz, C. A., Chen, L. X. & Young, L. (2011). *Rev. Sci. Instrum.* **82**, 073110.

Navirian, H., Shayduk, R., Leitenberger, W., Goldshteyn, J., Gaal, P. & Bargheer, M. (2012). *Rev. Sci. Instrum.* **83**, 063303.

Nozawa, S., Adachi, S., Takahashi, J., Tazaki, R., Guérin, L., Daimon, M., Tomita, A., Sato, T., Chollet, M., Collet, E., Cailleau, H., Yamamoto, S., Tsuchiya, K., Shioya, T., Sasaki, H., Mori, T., Ichiyanagi, K., Sawa, H., Kawata, H. & Koshihara, S. (2007). *J. Synchrotron Rad.* **14**, 313–319.

Schick, D., Herzog, M., Wen, H. D., Chen, P., Adamo, C., Gaal, P., Schlom, D. G., Evans, P. G., Li, Y. L. & Bargheer, M. (2014). *Phys. Rev. Lett.* **112**, 097602.

Wen, H. D., Chen, P., Cosgriff, M. P., Walko, D. A., Lee, J. H., Adamo, C., Schaller, R. D., Ihlefeld, J. F., Dufresne, E. M., Schlom, D. G., Evans, P. G., Freeland, J. W. & Li, Y. L. (2013). *Phys. Rev. Lett.* **110**, 037601.

Zhang, B. B., Sun, S. S., Sun, D. R. & Tao, Y. (2014). *Rev. Sci. Instrum.* **85**, 096110.